BER the international journal of bridge engineering management and research

Capacity Evaluation for the End Region of Concrete Barriers under Lateral Loading

Ran Cao[1,*]; Wanting Wang[2]; Anil Kumar Agrawal[3]; Sherif El-Tawil[4]; Yuan Chen[5] and Waider Wong[6]

Submitted: 15 September 2025 **Accepted:** 21 December 2025 **Publication date:** 10 April 2026

DOI: 10.70465/ber.v3i2.67

Abstract: Per current design specifications, bridge barriers must be designed to resist the lateral impact from errant trucks with specified weights and speeds. While most past research has focused on the performance of the interior regions of barriers, the structural capacity of the edge region remains less understood. Unlike the interior, the edge of a barrier is limited by its unsupported edge boundary, making it more vulnerable to damage. To address this gap, high-fidelity computational simulation models are used to study the resistance mechanisms of barrier edges subjected to pushover loads. The results are synthesized into design equations to estimate both flexural and punching shear capacity of the barrier edge. The findings provide new insight into barrier edge behavior and offer guidance for potential updates to current design specifications.

Author keywords: Concrete barrier; edge region; modified yield line method

Notation

The following symbols are used in this paper:

b_0	perimeter of the punching shear zone
d	effective depth of the parapet
D	parapet thickness
f_c'	compressive strength of concrete
H	height of the wall/barrier
H_e	height of load application (effective loading height)
H_1	height of the loading area (for punching shear)
L_c	critical length of yield line failure pattern
L_t	longitudinal length of distribution of impact force (loading length)
M_c	flexural resistance of cantilevered walls about an axis parallel to the longitudinal axis of the bridge
$M_{c,avg}$	average cantilever bending capacity of the barrier over its height
$M_{c,base}$	cantilever bending capacity of the barrier at its base
M_w	flexural resistance of the wall about its vertical axis
R_w	total transverse resistance of the railing
V_c	punching shear capacity of the barrier
x	variable length identifying the horizontal yield line extension
β	ratio of loading length to loading height used in punching shear calculation
λ_s	the size effect modification factor.

*Corresponding Author: Ran Cao. Email: rcao@hnu.edu.cn

[1]Associate Professor, College of Civil Engineering, Hunan University, Changsha 410082, China

[2]Research Assistant, College of Civil Engineering, Hunan University, Changsha 410082, China

[3]Professor, Dept. of Civil and Environmental Engineering, The City College of the City University of New York, New York, NY 10031

[4]Professor, Dept. of Civil & Environmental Engineering, University of Michigan, Ann Arbor, MI 48109

[5]Engineer, Hunan Architectural Design Institute Group Co., Ltd., Changsha 410082, China

[6]Engineer, Federal Highway Administration, Baltimore, MD 21201

Discussion period open till six months from the publication date. Please submit separate discussion for each individual paper. This paper is a part of the Vol. 3 of the International Journal of Bridge Engineering, Management and Research (© BER), ISSN 3065-0569.

Introduction

Reinforced concrete (RC) barriers are important protective structures for highway infrastructure. Section 13 of the AASHTO[1] specification requires that a barrier be designed to resist the demands generated by truck impact as a function of truck type, speed, and weight. Barrier capacity in the AASHTO[1] specification is computed using the yield line method (YLM), for which an assumed yield line mechanism is prescribed. Several researchers have criticized the prescribed yield line mechanism.[2–5] They noted that it may be quite different from that observed in actual accidents and experiments and could lead to unreasonable designs. To address this issue, several modified yield line mechanisms (MYLMs) were proposed by Jeon et al.,[2] Khederzadeh,[3] and Cao et al.[4] However, to date, there has not been a consensus on which YLM for concrete barriers is most representative of actual behavior.

Most of the previous studies focused on the interior region of the barrier. Studies on the end region of the barrier are limited. This is troublesome because the lateral resistance at the edge of the barrier is generally weaker than that of the interior region because the edge is unsupported. Khederzadeh[3] conducted one of the few static load tests on the end region of a concrete barrier. Based on their testing results, they proposed a new YLM to predict the flexural capacity of the barrier. However, the estimated barrier capacity from their method was only 62% of the test result per their report. Although this ensures safety, it represents an overly conservative prediction that forces the use of excessive materials to satisfy design requirements.

More recently, Steelman et al.[6] conducted both experimental and simulation studies on the damage mechanism of concrete barriers under lateral loading. The research focused on both interior and edge regions. Their tests at the edge region revealed severe damage to the deck overhang and localized fracture of the parapet under impact conditions. They proposed a MYLM based on the test results and accompanying simulation studies. Their study highlighted the significance of torsional effects in the barrier-deck system, although they did not account for that in their proposed design model.

Motivated by the lack of research data on this topic, this study uses high-fidelity computational simulation to investigate the behavior and failure mode of a barrier's end zone subjected to lateral loading. Both flexural and punching shear failure modes are considered, and design equations are developed to predict the flexural and punching shear capacities of the barrier.

Finite Element Model and Simulation Setup

Fig. 1a shows the general loading setup of the barrier model in LS-DYNA.[7] Based on the previous studies on truck impact with bridge barriers,[4,8,9], a quasi-static loading was applied at the upper portion of the parapet to simulate truck impact loads. In Fig. 1a, the steel loading plate has a vertical height of 80 mm, and the contact between the loading plate and the concrete wall was modeled via the *CONTACT_AUTOMATIC_SURFACE_TO_SURFACE command in LS-DYNA. As shown in Fig. 1a, the rebars and concrete were modeled separately, and their interaction was simulated using the *CONSTRAINED_BEAM_IN_SOLID command, assuming a perfect bond.

The detailing of the barrier is shown in Fig. 1b and Table 1, which is based on the standard drawings of the TL-4 and TL-5 barrier classes used by different State Departments of Transportation. This specific design configuration was selected because it is widely adopted in modern highway construction. Moreover, the vertical geometry represents the most fundamental cross-section for analysis, facilitating the clear identification of plastic hinge formations and yield line patterns. By varying the length of the loading plate (to simulate different loading conditions) and rebar strength (to model different strength conditions), a total of eight TL-4 cases and three TL-5 cases were considered in this work, as shown in Table 1. The strength of the concrete is 28 MPa for the deck and 25 MPa for the parapet. Nonlinear properties of the concrete and steel rebars in the parapet were simulated using material models *MAT_159 and *MAT_003 in LS-DYNA. The deck, however, was modeled as elastic to localize damage in the parapet and thus focus the study on only that aspect of behavior. The above modeling scheme was validated against multiple impact tests and shown to yield reasonable results, as outlined in Cao et al.[4,10].

Simulation Results

Fig. 2 shows the computed pushover curves for the first three TL-4 cases and the three TL-5 cases in Table 1. Pushover curves plot the applied force versus lateral displacement of the barrier computed at the loading height at the edge of the barrier. Also plotted in Fig. 2 are the calculated capacities computed using the yield line analysis per AASHTO[1] specifications (Eqs. (1) and (2)). It can be seen from Fig. 2 that AASHTO[1] specification results underestimate the capacity of TL-4 cases while overpredicting the capacity for TL-5

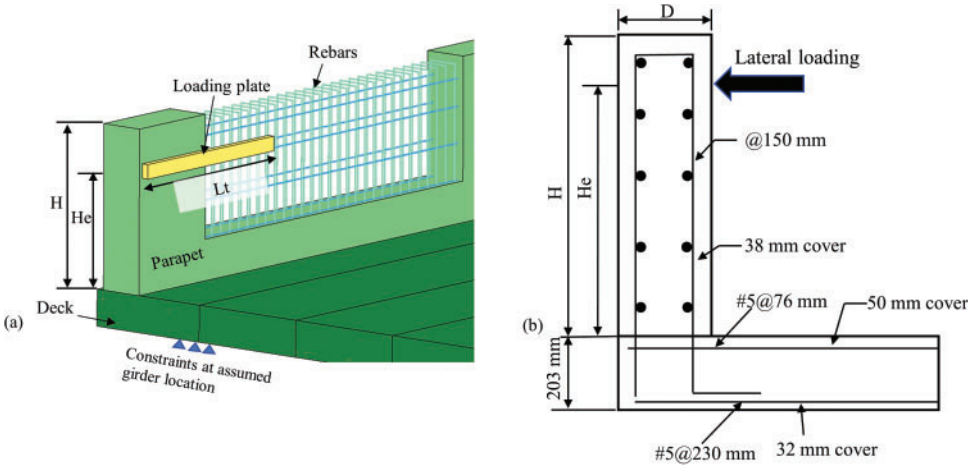

Figure 1. Finite element model of the concrete barrier

Table 1. Design parameters of the concrete barriers

Case	D (m)	H (m)	H_e (m)	L_t (m)	Longitudinal rebars		Stirrups	
					Diameter (mm)	Yield strength (MPa)	Diameter (mm)	Yield strength (MPa)
TL-4_1	0.25	0.91	0.68	1.07	10.16	415	9.53	485
TL-4_2	0.25	0.91	0.68	1.07	10.16	332	9.53	388
TL-4_3	0.30	0.91	0.68	1.07	10.16	415	9.53	485
TL-4_4	0.25	0.91	0.68	1.37	10.16	415	9.53	485
TL-4_5	0.25	0.91	0.68	1.68	10.16	415	9.53	485
TL-4_6	0.25	0.91	0.68	2.59	10.16	415	9.53	485
TL-4_7	0.25	0.91	0.68	2.90	10.16	415	9.53	485
TL-4_8	0.25	0.91	0.68	3.66	10.16	415	9.53	485
TL-5_1	0.29	1.07	0.86	2.44	12.70	415	12.70	485
TL-5_2	0.29	1.07	0.86	3.05	12.70	415	12.70	485
TL-5_3	0.29	1.07	0.86	3.66	12.70	415	12.70	485

Note: D = parapet thickness; H = barrier height; H_e = loading height.

cases, which casts doubt on the accuracy of the AASHTO[1] specification equations:

$$R_w = \left(\frac{2}{2L_c - L_t}\right)\left(M_w + \frac{M_c L_c^2}{H}\right) \quad (1)$$

$$L_c = \frac{L_t}{2} + \sqrt{\left(\frac{L_t}{2}\right)^2 + H\left(\frac{M_w}{M_c}\right)} \quad (2)$$

where H is the height of wall (m); L_c is the critical length of yield line failure pattern (m); L_t is the longitudinal length of distribution of impact force (m); R_w is the total transverse resistance of the railing (kN); M_c is the flexural resistance of cantilevered walls about an axis parallel to the longitudinal axis of the bridge (kN); and M_w is the flexural resistance of the wall about its vertical axis (kN·m).

To better understand the barrier responses, Fig. 3 shows the simulated damage pattern of the barrier when the pushover loading reached its peak value. As shown in Fig. 3, one horizontal and one diagonal yield line developed on the front face of the barrier, while a diagonal yield line formed on the back face. Similar damage patterns have been observed in the experimental tests by Steelman et al.[6], as shown in Fig. 4, where horizontal and diagonal flexural cracks were evident on both faces of the parapet.

To further examine the capacity calculation specified in AASHTO[1] specifications, Fig. 5 illustrates the yield line mechanism prescribed in Section 13, which adopts a half-V-shaped cracking pattern to compute the flexural capacity of the barrier. It can be seen from Fig. 5 that the assumed damage pattern in the current design code is quite different from the simulation results in Fig. 3 and the experimental observations in Fig. 4. In particular, the AASHTO[1] specifications model neglects the horizontal yield line at the base of the barrier as well as the cracking on the back of the barrier.

MYLM for the End Region of the Barrier

To address the discrepancy mentioned above, an MYLM is proposed in Fig. 6, in which yield lines on both the front and back faces of the barrier are considered.

As shown in Fig. 6, the following assumptions are adopted based on the simulation results:

- On the front face of the parapet, the diagonal yield line forms an angle of 45° with the horizontal axis and is perpendicular to the diagonal yield line on the back face.
- The length of the horizontal yield line at the parapet base exceeds the length of the loading plate, L_t, and can be determined through partial differentiation to minimize it with respect to the additional variable, x, per the upper bound yield line theory.
- The influence of loading height on the yield line pattern is considered by multiplying the calculated R_w with a ratio of H/H_e[5].

The general procedure of the derivation for the capacity of the parapet is similar to that in Hirsch (1978), and the final expression for the capacity equation and length of the yield lines are shown in Eqs. (3)–(5). The detailed derivation of the MYLM based on the energy method is shown in the appendix.

$$R_w = \frac{H}{H_e}\left[\left(\frac{x+3H}{x+H}\right)\left(\frac{M_w}{2H} + \frac{1}{2}M_c\right) + \frac{M_c\,(L_t + x)}{H}\right] \quad (3)$$

$$L_c = L_t + H + x \quad (4)$$

$$x = H\sqrt{1 + \frac{M_w}{M_c H}} - H \quad (5)$$

As shown in Fig. 2, the calculated flexural capacity using the proposed method (MYLM) matched the pushover simulations much better than that from the AASHTO [1] specifications method.

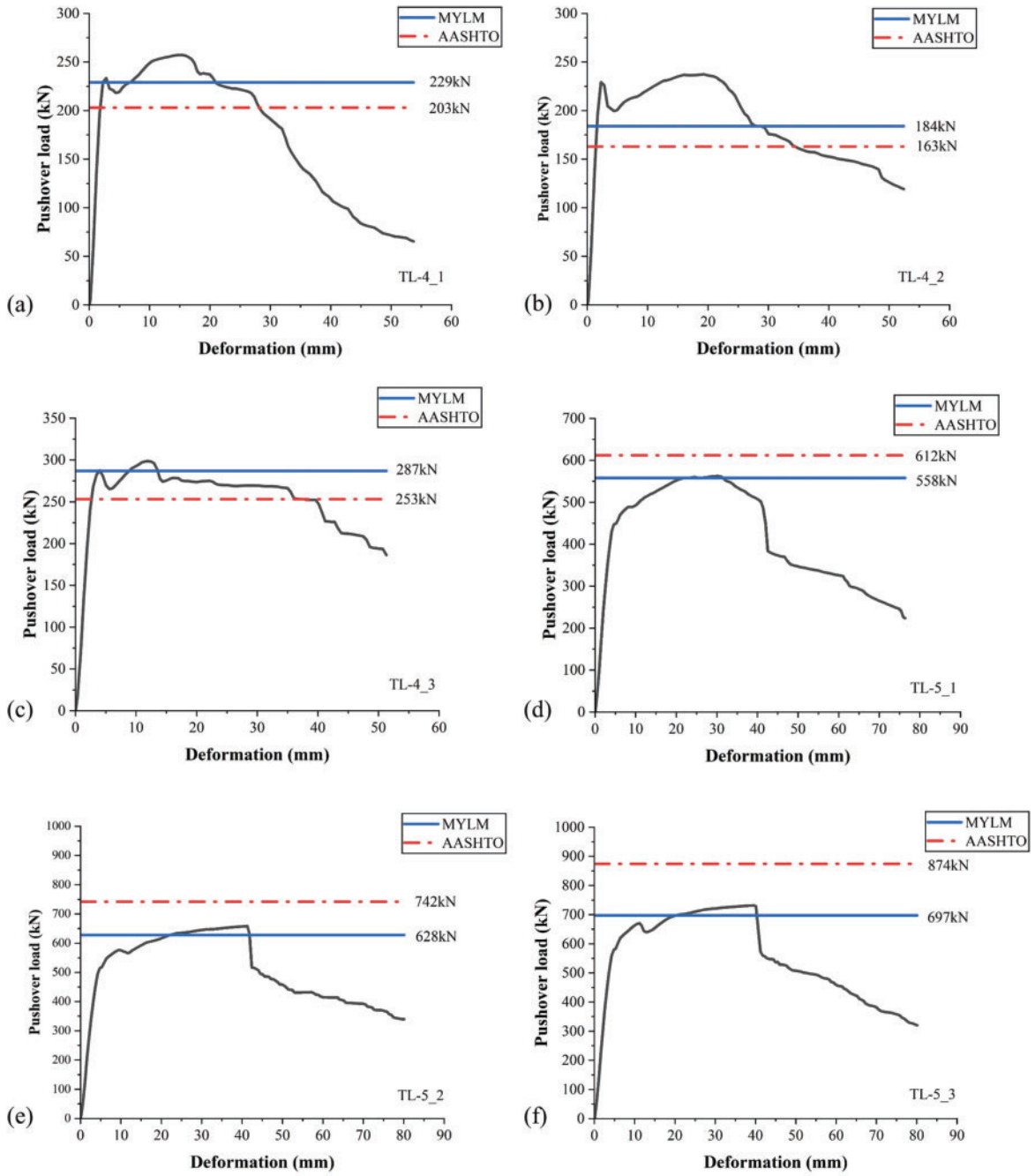

Figure 2. Simulated pushover curves for TL-4 and TL-5 barriers: (a) TL-4_1; (b) TL-4_2; (c) TL-4_3; (d) TL-5_1; and (e) TL-5_2; (f) TL-5_3

It should be noted that the National Cooperative Highway Research Program (NCHRP) report by Steelman et al.[6] also studied the assessment of the lateral capacity of the concrete barrier when loaded at its end region. The assumed yield line mechanisms in their model are illustrated in Fig. 7, which also consists of three yield lines, that is, one horizontal line at the base of the barrier, one diagonal crack on the front face of the barrier, and one vertical crack on the back of the barrier. Different from our model shown in Fig. 6, (1) the length of the horizontal yield line is fixed as half of the loading length, that is, $0.5L_t$; (2) the crack at the back of the barrier was assumed to be vertical, while in our model it is assumed to be diagonal. Their derived equations for the barrier's flexural capacity and critical length for the yield line pattern are shown in Eqs. (6) and (7):

$$R_w = \frac{H}{H_e}\left(\frac{8M_w}{L_c - 0.5L_t} + \frac{4M_{c,avg}}{H}(L_c - 0.5L_t) + \frac{2M_{c,base}L_t}{H}\right)\left(3 + \frac{L_c - L_t}{L_c - 0.5L_t}\right)^{-1} \tag{6}$$

$$L_c = \frac{5M_{c,avg}L_t + \sqrt{M_{c,avg}\left(M_{c,avg}L_t^2 + 4M_{c,base}L_t^2 + 128HM_w\right)}}{8M_{c,avg}} \tag{7}$$

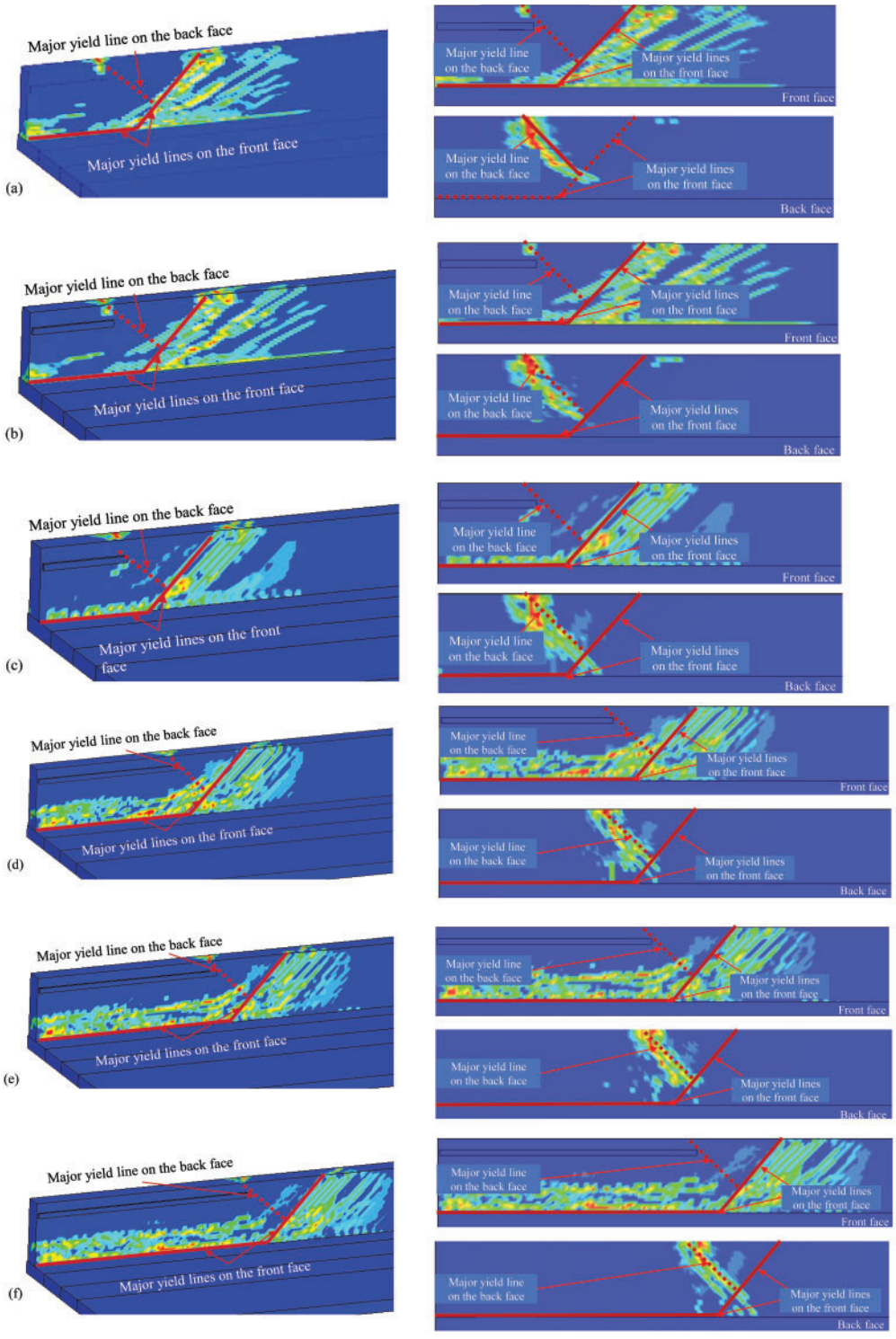

Figure 3. Damage mode of TL-4 and TL-5 barriers from pushover simulations: (a) TL-4_1; (b) TL-4_2; (c) TL-4_3; (d) TL-5_1; (e) TL-5_2; and (f) TL-5_3

where H is the height of wall (m); H_e is the height of load application (m); L_c is the critical length of yield line failure pattern (m); L_t = is the longitudinal length of distribution of impact force (m); R_w = is the total transverse resistance of the railing (kN); $M_{c,avg}$ = is the average cantilever bending capacity of the barrier over its height (kN); $M_{c,base}$ = is the cantilever bending capacity of the barrier at its base (kN); and M_w is the flexural resistance of the wall about its vertical axis (kN·m).

To compare the accuracy and effectiveness of the three analytical models, Fig. 8 shows the calculated flexural capacity of the 11 barriers in Table 1 computed using the AASHTO[1] specifications, MYLM, and NCHRP methods. It can be observed from Fig. 8 that the NCHRP results

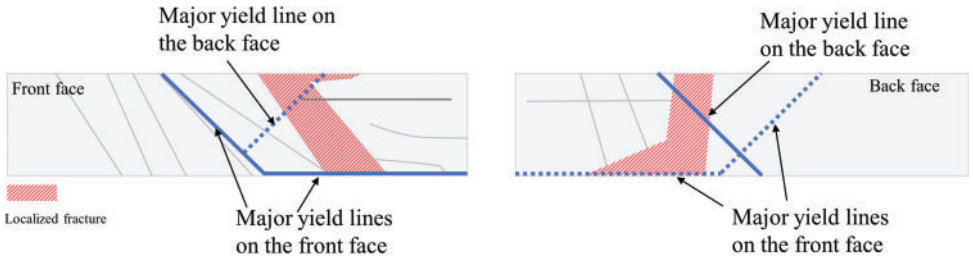

Figure 4. Cracking patterns of the barrier observed in a field impact testing (recreated from[6])

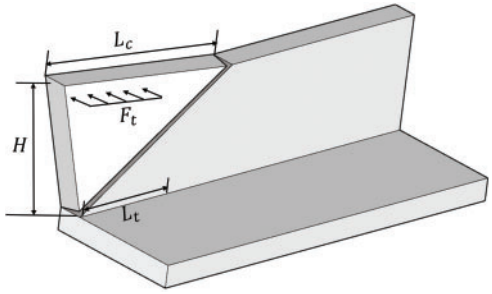

Figure 5. Yield line pattern used in the current AASHTO[1] specifications.

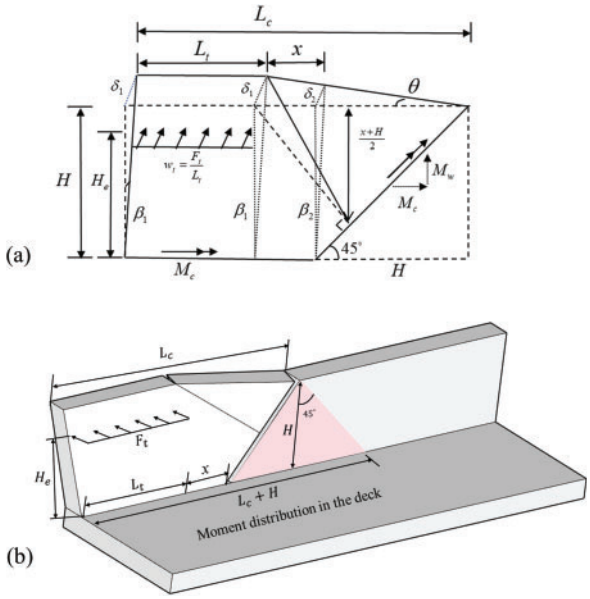

Figure 6. Modified yield line pattern for the end region of the barrier: (a) schematic front view and (b) 3D view

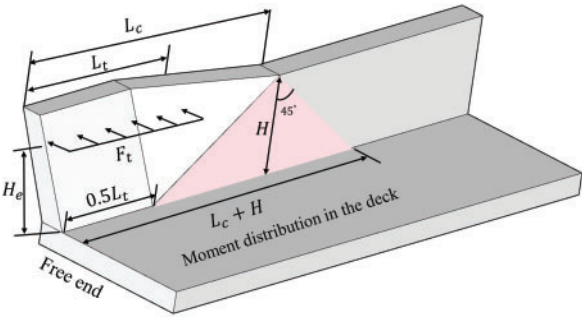

Figure 7. Yield line pattern proposed in Steelman et al.[6]

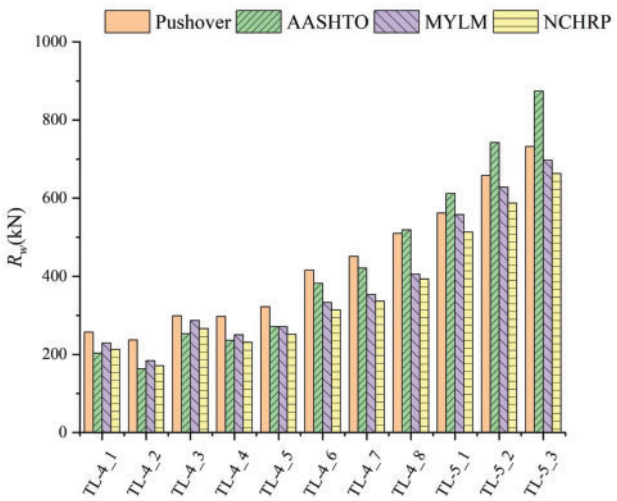

Figure 8. Comparison of flexural capacity of the barrier using different models

were slightly lower (with an average difference of 6%) than those of MYLM, and both of them were below the pushover simulation results. For barriers with longer loading lengths (TL-4_8 and all TL-5 cases), however, the AASHTO[1] specifications method overestimated the flexural capacity relative to the pushover simulations, potentially resulting in unsafe designs.

Figs. 9 and 10 also illustrate the relationship between R_w and L_t for different YLMs, where M_c, M_w, and H are considered as fixed (from cases TL-4_1 and TL-5_1). It can be seen from these comparisons that, as L_t increases, R_w predicted by the AASHTO[1] specifications method increases at a faster rate than those from MYLM and NCHRP. This behavior explains the overprediction of the AASHTO method for cases with longer loading lengths, such as the TL-5 barriers.

Punching shear capacity is not addressed in the current AASHTO[1] specification. Since this is a viable failure mode as discussed in Cao et al.[10], punching shear capacity is computed as shown in Fig. 11 and specified in ACI[11].

$$V_c = \left(2 + \frac{4}{\beta}\right)\lambda_s \sqrt{f_c'} b_0 d \tag{8}$$

$$\beta = \frac{L_t}{H_1} \tag{9}$$

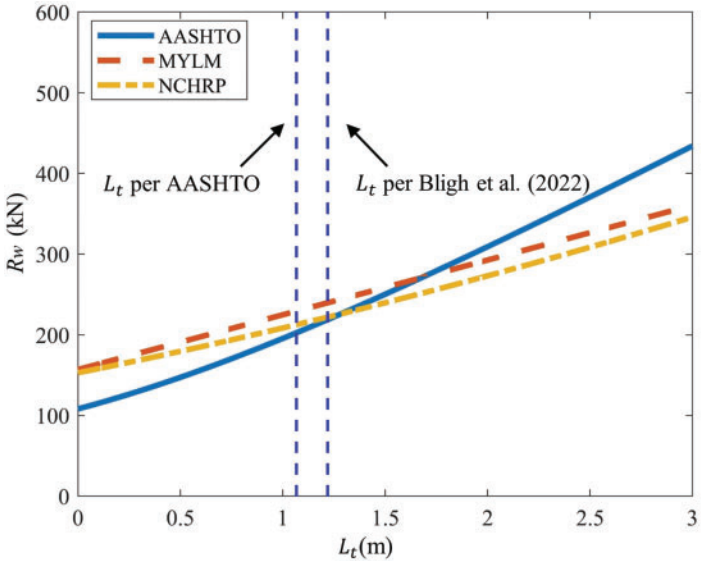

Figure 9. Effect of the loading length (L_t) on flexural capacity of the TL-4 barrier

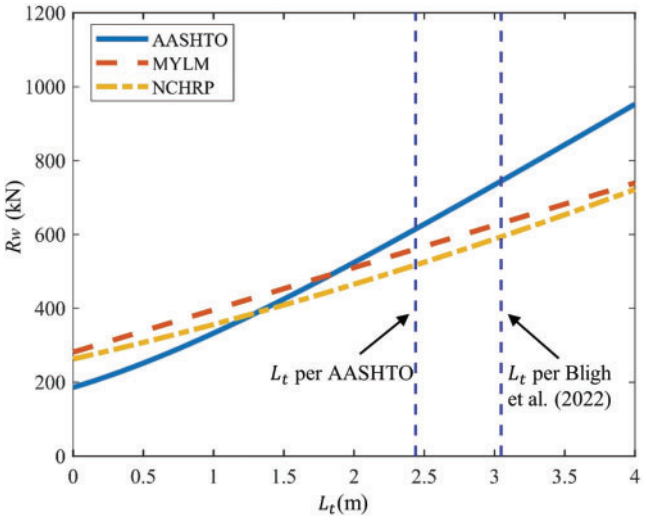

Figure 10. Effect of L_t on flexural capacity of the TL-5 barrier

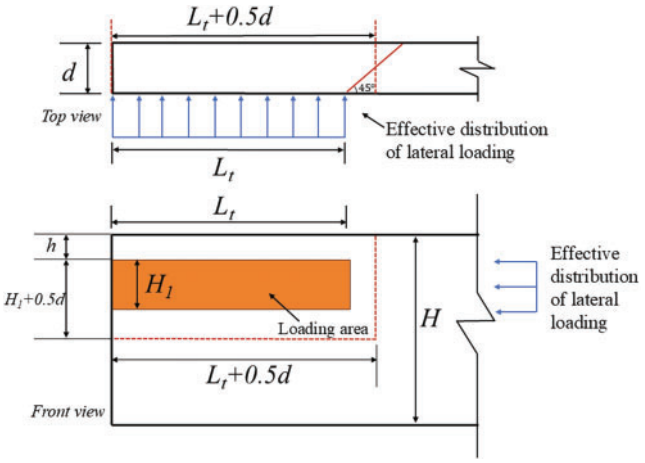

Figure 11. Illustration of the idealized punching shear scheme for the end region of the parapet

$$\lambda_s = \sqrt{\frac{2}{1+\frac{d}{10}}} \leq 1.0 \tag{10}$$

where V_c is the punching shear capacity of the barrier; f_c' is the compressive strength of the concrete; b_o is the perimeter of the punching shear zone; d is the effective depth of the parapet; L_t is the length of the applied loading; H_1 is the height of the loading area; and λ_s is the size effect modification factor.

Based on the punching shear scheme in Fig. 11 and Eqs. (8) and (9), the punching shear capacity of the barrier is calculated and shown in Table 2. Clearly, the punching shear capacities for all cases are higher than their flexural capacities, indicating that flexural failure is the dominant failure mode in this case.

In addition to the barrier capacity, Fig. 12 shows the comparisons of the critical length of the yield line pattern, L_c, predicted by different models. It can be seen from Fig. 12 and Table 3 that MYLM gives a longer L_c than that from AASHTO[1] specifications and NCHRP (with an average increase of 33%) and shows better agreement with the simulation results. The results from AASHTO[1] specifications and NCHRP were close (with an average difference of 7%). The longer and more accurate L_c predicted by MYLM implies that, for deck design, the applied lateral load and bending moment are distributed over a much wider area in the deck, leading to more economical design outcomes, as illustrated in Fig. 6.

Critique of the AASHTO Equation

Based on the preceding discussion analyzing specific TL-4 and TL-5 RC parapet designs, the current design equation

Table 2. Calculated flexural and shear capacity of concrete barrier by different models

Case	AASHTO (kN)	MYLM (kN)	NCHRP (kN)	Punching shear (kN)	Simulation (kN)
TL-4_1	203	229	213	433	257
TL-4_2	163	184	171	433	237
TL-4_3	253	287	266	564	299
TL-4_4	236	250	231	487	297
TL-4_5	271	271	251	543	322
TL-4_6	382	333	314	716	416
TL-4_7	421	353	336	774	451
TL-4_8	519	405	393	921	510
TL-5_1	612	558	513	846	562
TL-5_2	742	628	587	987	658
TL-5_3	874	697	663	1,129	732

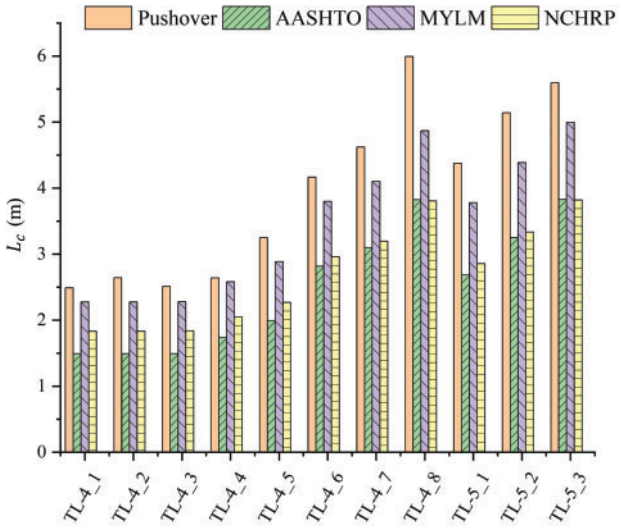

Figure 12. Comparison of the critical length of the yield line pattern using different models

Table 3. Comparison of critical length of yield line pattern of the barrier by different models

Barrier type	Case	Pushover (m)	AASHTO (m)	MYLM (m)	NCHRP (m)
TL-4	TL-4_1	2.49	1.49	2.28	1.83
	TL-4_2	2.64	1.49	2.28	1.83
	TL-4_3	2.51	1.50	2.28	1.84
	TL-4_4	2.64	1.74	2.58	2.05
	TL-4_5	3.25	1.99	2.89	2.27
	TL-4_6	4.17	2.82	3.80	2.96
	TL-4_7	4.62	3.10	4.11	3.20
	TL-4_8	5.99	3.82	4.87	3.81
TL-5	TL-5_1	4.38	2.68	3.78	2.86
	TL-5_2	5.14	3.25	4.39	3.33
	TL-5_3	5.60	3.83	5.00	3.82

for barrier capacity in AASHTO[1] specifications exhibits several shortcomings within the context of the configurations investigated:

1) The assumed damage mode does not match the simulation and experimental results observed for these specific barriers. Specifically, yield lines at the base and back face of the parapet, clearly identified in tests and simulations, are ignored in the AASHTO[1] specifications method.
2) By comparing the simulation results with the analytical solutions for the selected cases, the AASHTO[1] specifications equation tends to overestimate the capacity of the specific TL-5 barrier design studied, which could lead to unconservative designs for similar geometries. The major reason for this deficiency is that the effects of the loading length on the calculated barrier capacity are not reasonably accounted for in this context.

It should be acknowledged that these outcomes and limitations are identified based on the specific barrier geometries and reinforcement details considered in this study. The performance and failure mechanisms might differ for other RC barriers. Therefore, further research investigating a wider variety of barrier configurations is recommended to fully assess the range of applicability of the AASHTO specifications.

Conclusions

This paper investigated the damage mechanism of the specific continuous RC barriers subject to lateral loading applied at the end region of the parapet. Based on validated pushover simulations, design schemes and equations were proposed for estimating the flexural and punching shear capacity of the barrier. Compared with the YLM in the current design guidelines, the proposed MYLM better captured the observed flexural failure patterns and provided more

realistic predictions of barrier capacity. While the results from the MYLM were generally consistent with those from the recent NCHRP equations, the yield line patterns derived from the MYLM were more physically representative, and the critical yield line lengths obtained were longer than those predicted by the NCHRP method, which also better matched the simulation results.

Overall, the MYLM offers a more rational basis for assessing barrier performance at the end region under lateral loads. However, further research, including quasi-static testing and evaluation of the deck overhang's role in system behavior, and investigation of a wider range of barrier geometries, is needed to fully validate and refine the proposed design method and assess its applicability to other parapet types.

Appendix—Development of MYLM

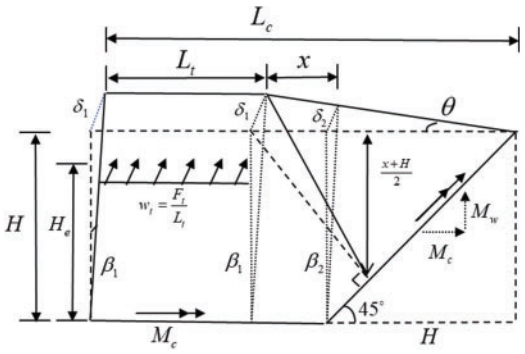

External work:

$$W = F_t \delta_1 \frac{H_e}{H} \tag{A1}$$

Internal work:

$$U_w = \left(1 + \frac{x+H}{2H}\right) M_w \theta \tag{A2}$$

$$U_c = M_c L_t \beta_1 + M_c x \frac{\beta_1 + \beta_2}{2} + M_c x \frac{\beta_1 + \beta_2}{2} + M_c \beta_2 \left(\frac{x+H}{2} - x\right) + M_c H \beta_2 \tag{A3}$$

$$U_w + U_c = \left(\frac{x+3H}{2H}\right) M_w \theta + M_c L_t \beta_1 + M_c x(\beta_1 + \beta_2) + M_c \beta_2 \left(\frac{3H-x}{2}\right) \tag{A4}$$

Since external work equals internal work, we have

$$F_t \delta_1 \frac{H_e}{H} = \left(\frac{x+3H}{2H}\right) M_w \theta + M_c L_t \beta_1 + M_c x\,(\beta_1 + \beta_2) + M_c \beta_2 \left(\frac{3H-x}{2}\right) \tag{A5}$$

$$\theta = \frac{\delta_1}{x+H} \tag{A6}$$

$$\beta_1 = \frac{\delta_1}{H} \tag{A7}$$

$$\beta_2 = \frac{\delta_2}{H} = \frac{\delta_1}{x+H} \tag{A8}$$

Substituting Eqs. (A6), (A7), and (A8) into (A5), we have

$$F_t = \frac{H}{H_e}\left[\left(\frac{x+3H}{x+H}\right)\left(\frac{M_w}{2H} + \frac{1}{2}M_c\right) + M_c \frac{L_t + x}{H}\right] \tag{A9}$$

The maximum value of F_t with respect to a change in x occurs when $\frac{d(F_t)}{d(x)} = 0$; this minimization gives a quadratic equation that can be solved explicitly to find the critical length, x, as

$$x = H\sqrt{1 + \frac{M_w}{M_c H}} - H$$

The total length of the yield line pattern is as follows:

$$L_c = L_t + H + x$$

Knowing that $F_{t,min} = Rw$, the minimum nominal resistance of the barrier wall system can be written as

$$R_w = \frac{H}{H_e}\left[\left(\frac{x+3H}{x+H}\right)\left(\frac{M_w}{2H} + \frac{1}{2}M_c\right) + M_c \frac{L_t + x}{H}\right]$$

References

[1] AASHTO. *AASHTO LRFD Bridge Design Specifications*. 9th ed. Washington, D.C.: American Association of State Highway and Transportation Officials; 2020.

[2] Jeon SJ, Choi MS, Kim YJ. Failure mode and ultimate strength of precast concrete barrier. *Aci Struct J*. 2011;108(1):99. doi:10.14359/51664207.

[3] Khederzadeh H. Development of innovative designs of bridge barrier system incorporating reinforcing steel or GFRP bars. Doctoral dissertation, Ph. D. Thesis. Ryerson University, Toronto, Ontario, Canada; 2014.

[4] Cao R, Agrawal AK, El-Tawil S, Wong W. Numerical studies on concrete barriers subject to MASH truck impact. *J Bridge Eng*. 2020;25(7):04020035. doi:10.1061/(asce)be.1943-5592.0001570.

[5] Loken AE, Steelman JS, Rosenbaugh SK, Faller RK, Holt JM. Comparison of modified yield-line and punching shear capacities for concrete traffic barriers and bridge rails. *Transp Res Rec*. 2021;2675(12):689–701. doi:10.1177/03611981211031222.

[6] Steelman JS, Loken AE, Faller RK, et al. MASH railing load requirements for bridge deck overhang (No. NCHRP Project 12-119); 2023. doi:10.17226/27422.

[7] Hallquist JO. LS-DYNA theory manual. *Livermore Softw Technol Corp*. 2006;3:25–31.

[8] Bligh RP, Briaud JL, Abu-Odeh A, Saez DO, Maddah LS, Kim KM. Design guidelines for test level 3 through test level 5 roadside barrier systems placed on mechanically stabilized earth retaining walls (No. NCHRP Project 22–20 (02)); 2022. doi:10.17226/26580.

[9] Cao R, El-Tawil S, Agrawal A, Wong W. Demand model for concrete barriers subject to tractor tanker-trailer impact. *Int J Bridge Eng Manag Res*. 2024;1(1):21424006–21424001. doi:10.70465/ber.v1i1.3.

[10] Cao R, El-Tawil S, Agrawal AK, Wong W. Performance and capacity assessment of concrete barriers subject to lateral loading. *J Bridge Eng*. 2021;26(12):04021090. doi:10.1061/(asce)be.1943-5592.0001789.
[11] ACI. *Building Code Requirements for Structural Concrete (ACI 318-19) and Commentary (ACI 318R-19)*. Farmington Hills, MI: American Concrete Institute; 2019.